Catalysis Today 175 (2011) 209–215

Contents lists available at ScienceDirect

Catalysis Today

journal homepage: www.elsevier.com/locate/cattod

PMMA-templating preparation and catalytic properties of high-surface-area three-dimensional macroporous La_2CuO_4 for methane combustion

Jing Yuan, Hongxing Dai*, Lei Zhang, Jiguang Deng, Yuxi Liu, Han Zhang, Haiyan Jiang, Hong He

Laboratory of Catalysis Chemistry and Nanoscience, Department of Chemistry and Chemical Engineering, College of Environmental and Energy Engineering, Beijing University of Technology, Beijing 100124, PR China

ARTICLE INFO

Article history:
Received 15 October 2010
Received in revised form 23 March 2011
Accepted 6 April 2011
Available online 14 May 2011

Keywords:
Perovskite-like oxide catalyst
Three-dimensional macroporous lanthanum cuprate
Low-temperature reducibility
Methane combustion
Hard-templating strategy

ABSTRACT

The three-dimensional (3D) macroporous orthorhombically crystallized perovskite-like oxides La_2CuO_4 were prepared using the polymethyl methacrylate (PMMA) microsphere-templating strategy with nitrates of lanthanum and copper as metal source and a mixed solution of methanol and ethylene glycol as solvent in the absence or presence of citric acid and after calcination at various atmospheres. The as-prepared materials were characterized by means of X-ray diffraction, N_2 adsorption-desorption, scanning electron microscopy, X-ray photoelectron spectroscopy, and hydrogen temperature-programmed reduction. Catalytic activities of the materials were evaluated for the combustion of methane. The catalyst (La_2CuO_4-1) prepared with PMMA and citric acid possessed a 3D ordered macroporous (3DOM) structure and a surface area up to 46 m^2/g, whereas the one (La_2CuO_4-2) prepared with PMMA but without citric acid exhibited a 3D wormhole-like macroporous structure and a surface area of 39 m^2/g. There was the presence of a trace amount of $La_2O_2CO_3$ phase in the La_2CuO_4-1 and La_2CuO_4-2 catalysts. The calcination procedure (first in N_2 flow at 700 °C and then in air flow at 300 and 800 °C, respectively) was crucial in forming the 3D porous structure of La_2CuO_4. The as-obtained catalysts had overstoichiometric oxygen. The La_2CuO_4-1 catalyst showed better low-temperature reducibility than the La_2CuO_4-2 and La_2CuO_4-Citrate (derived from the conventional citric acid-complexing route) catalysts. The 3D porous La_2CuO_4 materials performed well in catalyzing the oxidation of methane, with the La_2CuO_4-1 catalyst showing the best performance (the temperature for 90% CH_4 conversion = 672 °C (reaction rate = ca. 40 mmol/(g h)) at CH_4/O_2 molar ratio = 1/10 and space velocity = 50,000 mL/(g h). It is concluded that the excellent catalytic performance of La_2CuO_4-1 was mainly related to the higher surface area, better low-temperature reducibility, and 3DOM architecture.

1. Introduction

Among the catalysts used for the combustion of methane, perovskite-type oxides (ABO_3) and perovskite-like oxides (A_2BO_4) show promising catalytic performance and good thermal stability [1,2]. Such a characteristic renders these materials applicable in catalyzing the reactions involving high temperatures. Catalytic activities of the A_2BO_4 are associated with a number of factors, such as surface area, crystal structure, oxygen nonstoichiometry, particle morphology or even crystal type (single- or polycrystal), which are often determined by the preparation method adopted. Surface areas of the A_2BO_4 materials prepared through the citric acid complexing [3] and solid-state reaction [4] pathways, however, are usually low (<10 m^2/g) due to their sintering at high temperatures (>800 °C) for the formation of the single-phase perovskite-like crystal phase. Therefore, it is highly desirable to develop an effective strategy for controlled preparation of perovskite-like oxides with porous structures and high surface areas.

In the past years, the colloidal crystal templating method has been used to generate three-dimensional (3D) ordered macroporous (3DOM) materials, such as spinel-type oxides MFe_2O_4 (M = Zn, Ni, Co) [5], $ZnAl_2O_4$ and $ZnCr_2O_4$ [6], perovskite-type oxides $LaAlO_3$ and $LaMnO_3$ [6], $La_{1-x}Sr_xFeO_{3-\delta}$ [7], and $La_{0.7}Ca_{0.3}MnO_3$ [8], in which the colloidal crystal template used was poly(methyl methacrylate) (PMMA) or polystyrene microspheres. These investigations revealed that pore structures of the as-fabricated mixed oxides were significantly destroyed at a calcination temperature above 800 °C, resulting in a remarkable drop in surface area. To the best of our knowledge, no reports on the preparation and catalytic utilization of 3DOM-structured A_2BO_4 materials have been seen in the literature.

Previously, we fabricated a number of 3DOM materials (e.g., MgO [9], γ-alumina [10], ceria–zirconia [9], and silica [10]) via the PMMA-templating route and numerous perovskites and

* Corresponding author. Tel.: +86 10 6739 6118; fax: +86 10 6739 1983.
E-mail address: hxdai@bjut.edu.cn (H. Dai).

0920-5861/$ – see front matter © 2011 Elsevier B.V. All rights reserved.
doi:10.1016/j.cattod.2011.04.013

related compounds (e.g., $La_{1-x}Sr_xMO_3$ (M = Co, Mn) [11,12], $La_{1-x}Sr_xM_{1-y}Fe_yO_3$ (M = Co, Mn) [13], $La_{2-x}Sr_xCuO_4$ [14], and $NdSrCu_{1-x}Co_xO_{4-\delta}$ and $Sm_{1.8}Ce_{0.2}Cu_{1-x}Co_xO_{4+\delta}$ [15]) via the citric acid complexing and/or hydrothermal routes, and investigated the catalytic behaviors of the mentioned mixed oxides for the oxidation of volatile organic compounds [11–13] and methane [14,15]. It was observed that $La_{2-x}Sr_xCuO_4$ (x = 0, 0.4) crystallites with rod-like morphologies performed well in catalyzing the combustion of methane [14]. Recently, we have extended our attention to the catalysis of 3DOM-structured perovskite-like oxides in the oxidation of hydrocarbons. Herein, we report the controlled making and catalytic performance of La_2CuO_4 with 3D macroporous architectures and high surface areas for methane combustion.

2. Experimental

2.1. Catalyst preparation

The 3D macroporous La_2CuO_4 catalysts were prepared using the PMMA-templating strategy. In a typical preparation, 2.1 g of $La(NO_3)_3{\cdot}6H_2O$, 0.6 g of $Cu(NO_3)_2{\cdot}3H_2O$, and 2.0 g of citric acid were added to a beaker containing a mixture of 8 mL of methanol and 17 mL of ethylene glycol (EG). After stirring for 1 h, the mixed solution was transferred to a beaker containing 1.0 g of the colloidal crystal template PMMA microspheres. After being soaked for 5 h, the solid was first filtered under vacuum (ca. 0.07 MPa) and dried at room temperature (RT) for 12 h, and then transferred to a ceramic boat which was placed in a tubular furnace. The thermal treatment process was divided into two steps: (i) the solid was first calcined in a N_2 flow of 20 mL/min at a ramp of 1 °C/min from RT to 700 °C and kept at this temperature for 4 h, and then cooled to 50 °C in the same atmosphere; and (ii) after being purged in an air flow of 20 mL/min, the solid was heated in the same atmosphere at a ramp of 1 °C/min from RT to 300 °C and held at this temperature for 3 h, and then was calcined continuously at the same ramp from 300 to 800 °C and maintained at 800 °C for 5 h. The as-obtained 3DOM-structured catalyst was denoted as La_2CuO_4-1. When no citric acid was added but other parameters and calcination procedures were the same as those adopted for the preparation of La_2CuO_4-1, the obtained 3D macroporous catalyst was denoted as La_2CuO_4-2. For comparison purposes, we also adopted the citric acid-complexing method to prepare the nonporous La_2CuO_4 catalyst (denoted as La_2CuO_4-Citrate) that was obtained after calcination in air at 950 °C for 6 h [14]. All of the chemicals (Beijing Chemical Reagent Company) were in analytical grade and used without further purification.

2.2. Catalyst characterization

X-ray diffraction (XRD) patterns were recorded on a Bruker D8 Advance diffractometer with Cu Kα radiation and nickel filter (λ = 0.15406 nm), the operating voltage and current was 40 kV and 35 mA, respectively. The crystal phases were identified by referring to the corresponding data of JCPDS Database. Thermogravimetric analysis (TGA) and differential scanning calorimetric (DSC) analysis of the uncalcined catalysts were conducted in an air flow of 100 mL/min at a heating rate of 10 °C/min from RT to 900 °C on a SDT Q600 instrument (TA). BET (Brunauer–Emmett–Teller) surface areas of the catalysts were measured via N_2 adsorption at −196 °C on a Micromeritics ASAP 2020 analyzer with the catalysts being outgassed at 300 °C for 1 h under vacuum before measurement. The scanning electron microscopic (SEM) images of the catalysts were recorded on a Gemini Zeiss Supra 55 apparatus (operating at 10 kV). Transmission electron microscopic (TEM) images of the catalysts were obtained using the JEOL-2010 equipment (operating at 200 kV). X-ray photoelectron spectroscopy (XPS, VG CLAM 4 MCD analyzer) was used to determine the La 3d, Cu 2p, O 1s, and C 1s binding energies (BEs) of surface species with Mg $K\alpha$ ($h\nu$ = 1253.6 eV) as the excitation source. The instrumental resolution was 0.5 eV. Before XPS measurement, the catalyst was calcined in O_2 (flow rate = 20 mL/min) at 600 °C for 1 h and then cooled to RT. After such a pretreatment, the catalyst was mounted and transferred to the spectrometer in a transparent Glove Bag (Instruments for Research and Industry, USA) filled with helium. The catalyst was then outgassed in the preparation chamber (10^{-5} Torr) for 0.5 h and introduced into the analysis chamber (3×10^{-9} Torr) for spectrum recording. The C 1s signal at 284.6 eV was taken as a reference for BE calibration.

Hydrogen temperature-programmed reduction (H_2-TPR) experiments were carried out on a chemical adsorption analyzer (Autochem II 2920, Micromeritics). Before the TPR measurement, 0.02 g of the catalyst (40–60 mesh) was first treated in a helium flow of 30 mL/min at 300 °C for 0.5 h in a quartz fixed-bed U-shaped microreactor (i.d. = 4 mm). After cooling to RT in the same atmosphere, the pretreated catalyst was exposed to a flow (50 mL/min) of 5% H_2–95% Ar (v/v) mixture and heated at a ramp of 15 °C/min to 900 °C. The alteration in H_2 concentration of the effluent was monitored on-line by the chemical adsorption analyzer. The reduction band was calibrated against that of the complete reduction of a known standard of powdered CuO (Aldrich, 99.995%).

2.3. Catalytic evaluation

Catalytic activities of the samples were measured using a continuous flow fixed-bed quartz microreactor (i.d. = 4 mm) at atmospheric pressure. 0.05 g of the catalyst (40–60 mesh) diluted with 0.1 g of quartz sand (40–60 mesh) was loaded into the microreactor. The volumetric composition of the reactant mixture was 2% CH_4 + 20% O_2 + 78% N_2 (balance) and the total flow was 41.6 mL/min, thus giving a space velocity (SV) of ca. 50,000 mL/(g h). The effluent gases were analyzed on-line by a Shimadzu GC-14C gas chromatography equipped with a thermal conductivity detector and a 5 Å molecular sieve column. The balance of carbon in each run was estimated to be ca. 99.5%.

3. Results and discussion

3.1. Crystal phase, thermal stability and pore structure

Fig. 1 shows the XRD patterns of the catalysts prepared with PMMA and of the La_2CuO_4-Citrate catalyst derived from the citric acid-complexing route. By referring to the XRD pattern (JCPDS PDF# 82-2142) of the standard La_2CuO_4 sample, one can deduce that (i) the La_2CuO_4-Citrate catalyst was single-phase with an orthorhombic perovskite-like structure; and (ii) the La_2CuO_4-1 and La_2CuO_4-2 catalysts were mainly composed of the orthorhombic perovskite-like oxide phase and there was the presence of a trace amount of $La_2O_2CO_3$ impurity phase (JCPDS PDF# 22-0642), which might be generated via the interaction of carbon dioxide emitted from the oxidation of the PMMA template and lanthanum species derived from the decomposition of lanthanum precursor during the calcination processes.

Shown in Fig. 2 are the TGA/DSC profiles of the uncalcined La_2CuO_4 samples. From Fig. 2A, one can observe four weight loss steps: (i) a gradual small weight loss of ca. 4 wt% due to the removal of methanol and adsorbed water appeared below 79 °C; (ii) a relatively big weight loss (ca. 14 wt%) in the range of 79–147 °C, accompanying by the appearance of an endothermic peak at 116 °C, which was related to the reaction of EG with metal nitrate to produce metal glyoxylate ($[C_2H_2O_4]^{2-}$) and NO_x [5,6]; (iii) a small weight loss of ca. 11 wt% in the range of 147–257 °C

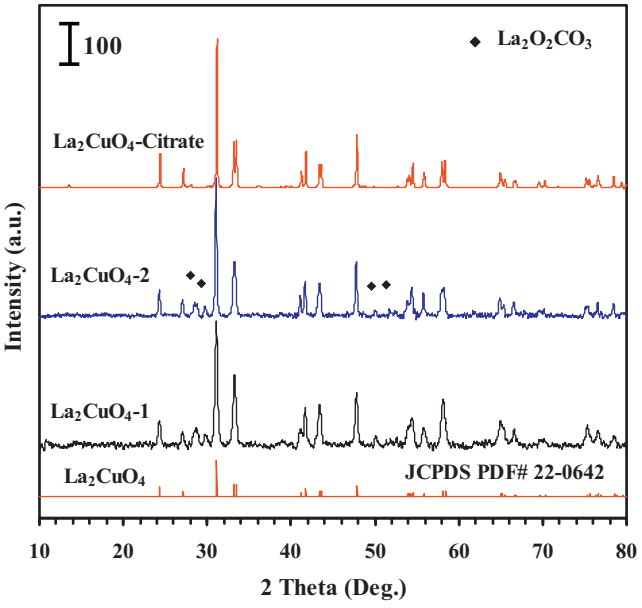

Fig. 1. XRD patterns of the as-prepared La_2CuO_4 catalysts.

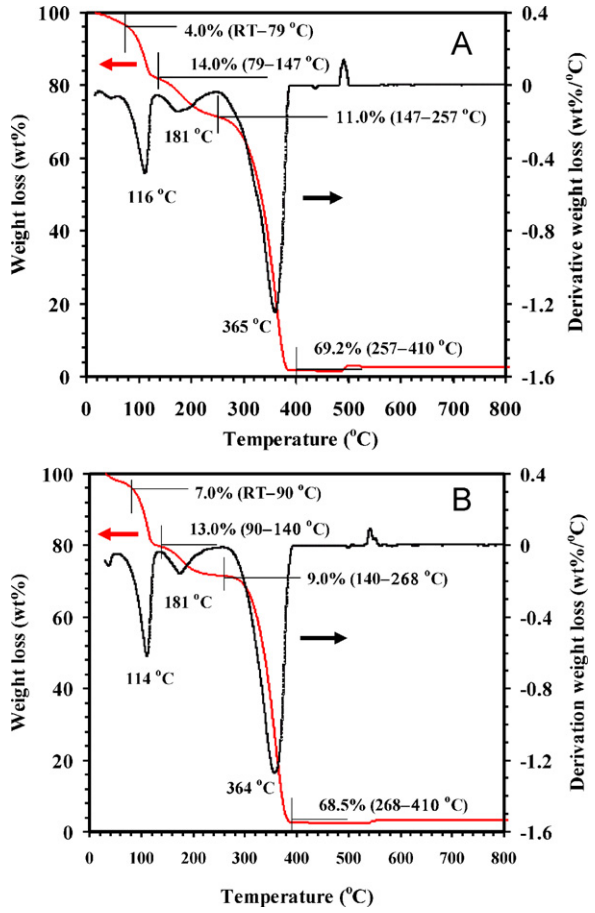

Fig. 2. TGA/DSC profiles of the uncalcined La_2CuO_4-1 (A) and La_2CuO_4-2 (B) samples.

and a corresponding weak endothermic signal centered at 181 °C was recorded, this weight loss might originate from the removal of the remaining EG (boiling point = ca. 197 °C), citric acid, and H_2O present in the sample; and (iv) a big weight loss (ca. 68.5 wt%) in the range of 257–410 °C, accompanying by the recording of a strong endothermic signal centered at 365 °C, such a big weight loss might be due to the oxidative decomposition of the PMMA template and metal glyoxylate [6]. The TGA/DSC profile of the uncalcined La_2CuO_4-2 sample (Fig. 2B) was rather similar to that of the uncalcined La_2CuO_4-1 sample, although the weight loss at each stage (as well as temperature of the corresponding endothermic signal) was slightly different. From Fig. 2, one can also observe a weight increase (ca. 0.4 wt%) around 500 °C, which might be due to the formation of a small amount of $La_2O_2CO_3$ phase [16,17]. The above results demonstrate that the PMMA template could be totally removed below 410 °C and the calcination temperature (800 °C) adopted in the present work was appropriate for the generation of single-phase perovskite-like oxide La_2CuO_4 materials, which was substantiated by the results of XRD investigations.

Fig. 3 shows the representative SEM and TEM images of the as-prepared La_2CuO_4 catalysts. The La_2CuO_4-1 catalyst derived in the presence of citric acid displayed a 3DOM structure with a pore-size range of 53–64 nm (Fig. 3a–c). The La_2CuO_4-2 catalyst derived without citric acid, however, showed a 3D wormhole-like macroporous structure with a pore-size range of 68–136 nm (Fig. 3d–f). Obviously, the introduction of citric acid during the fabrication process played an important role in the formation of 3DOM-structured La_2CuO_4. Citric acid could complex with the metal ions in the precursor solution, which would be beneficial for the formation of highly homogeneous metal complexes in an ideal metal stoichiometry required for perovskite-like oxide formation, hence favoring the generation of 3DOM structure during the calcination process [18].

It is worth mentioning that the calcination procedure (first in N_2 flow at 700 °C and then in air flow at 300 and 800 °C, respectively) was also important for 3DOM structure formation. The glassy temperature and decomposition temperature of PMMA is ca. 130 °C [5] and 290 °C [9], respectively. PMMA can be oxidized at ca. 370 °C [9]. In order to minimize the distortion of PMMA microspheres due to the softening, decomposition, and/or oxidation at higher temperatures, it is a better way to calcine the PMMA-containing metal precursors first in a N_2 flow at 700 °C (possibly leading to the carbonization of PMMA) and then in an air flow at 300 °C (possibly removing the carbon formed due to carbonization of PMMA) and 800 °C (leading to the formation of perovskite-like oxide phase). The introduction of citric acid to the metal precursor solution and the calcination of the PMMA-containing metal precursor in N_2 at 700 °C was favorable for the preservation of 3DOM structure, whereas the calcination of the citric acid-free PMMA-containing metal precursor in N_2 flow at 700 °C would lead to the collapse of 3DOM architecture and 3D wormhole-like macroporous La_2CuO_4 was generated as a result. It further confirms the important role of citric acid in forming the 3DOM-structured La_2CuO_4 materials.

As shown in Table 1, BET surface areas of the 3DOM-structured La_2CuO_4-1 and 3D wormhole-like macroporous La_2CuO_4-2 catalysts were 46 and 39 m^2/g, respectively, much higher than that (2.1 m^2/g) of the nonporous La_2CuO_4-Citrate catalyst. To the best of our knowledge, no reports have been seen so far in the literature on the preparation of La_2CuO_4 with such high surface areas (39–46 m^2/g).

3.2. Surface oxygen species, copper oxidation state, and reducibility

Illustrated in Fig. 4 are the O 1s and Cu $2p_{3/2}$ XPS spectra of the as-fabricated La_2CuO_4 catalysts. The curve-fitting strategy was used to make qualitative and quantitative analyses. The O 1s spectrum of La_2CuO_4-1, La_2CuO_4-2 or La_2CuO_4-Citrate could be decomposed into three components at BE = 528.6, 531.2, and 533.0 eV (Fig. 4A), attributable to the surface lattice oxygen (O_{latt}) species, adsorbed oxygen (O_{ads}, e.g. O^-, O_2^{2-} or O_2^-) species, and molecularly adsorbed water species [19], respectively. It has been

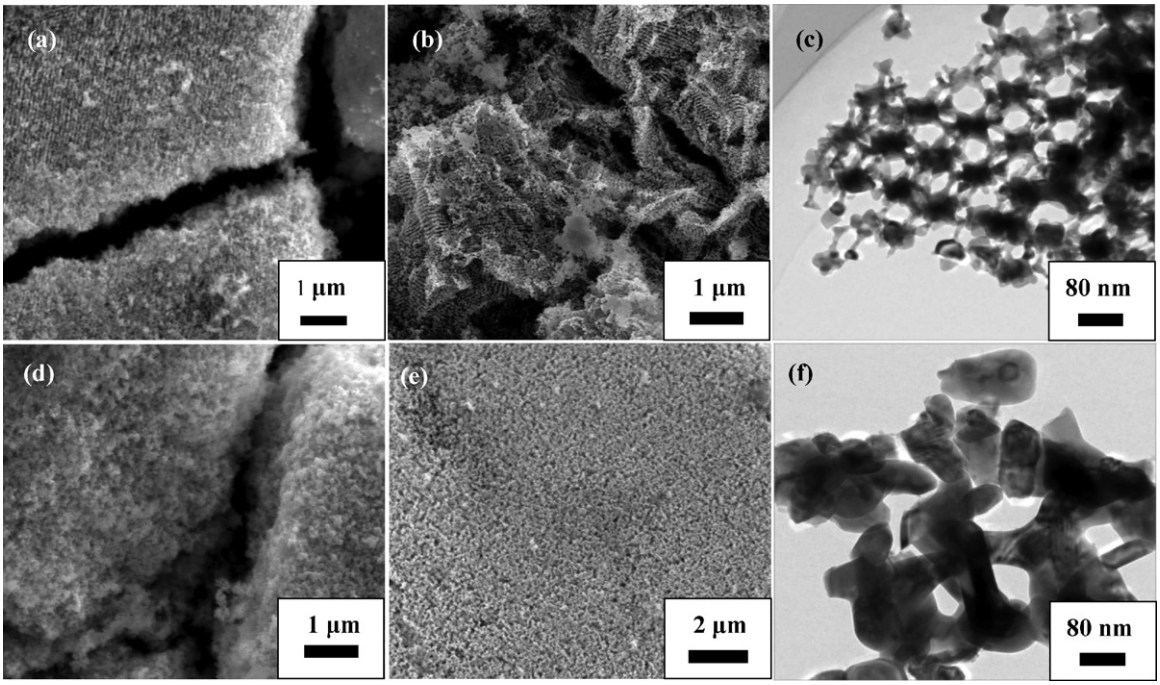

Fig. 3. SEM (a, b, d, e) and TEM (c, f) images of (a–c) La_2CuO_4-1 and (d–f) La_2CuO_4-2.

Table 1
BET surface areas, surface compositions, H_2 consumptions, and catalytic activities of the as-prepared La_2CuO_4 catalysts.

Catalyst	BET surface area (m^2/g)	Molar ratio[a] (mol/mol)		H_2 consumption[b] (mmol/g)		Catalytic activity	
		O_{ads}/O_{latt}	Cu^{3+}/Cu^{2+}	<500 °C	>500 °C	$T_{50\%}$ (°C)	$T_{90\%}$ (°C)
La_2CuO_4-1	46	2.41	0.21	2.04	0.67	560	672
La_2CuO_4-2	39	2.13	0.18	1.35	1.19	630	705
La_2CuO_4-Citrate	1.7	1.88	0.12	2.60	–	723	784

[a] The surface O_{ads}/O_{latt} and Cu^{3+}/Cu^{2+} molar ratios were estimated from the XPS spectra;
[b] The H_2 consumptions were calculated according to the H_2-TPR profiles.

generally accepted that the amount of O_{ads} species is intimately associated with the oxygen nonstoichiometry of a perovskite-type or perovskite-like oxide catalyst. As shown in Table 1, the surface O_{ads}/O_{latt} molar ratio (2.41) of La_2CuO_4-1 was much higher than that (2.13) of La_2CuO_4-2 and that (1.88) of La_2CuO_4-Citrate. From the Cu $2p_{3/2}$ XPS spectra (Fig. 4B), one can observe an asymmetrical main signal at BE = ca. 933 eV and shake-up satellites in the BE range of 938–947 eV. The main signal could be decomposed into two components at BE = 932.7–933.2 and 934.8 eV, assignable to Cu^{2+} [20] and Cu^{3+} [20,21], respectively. The appearance of shake-up satellites was an evidence for the presence of Cu^{2+}. The surface Cu^{3+}/Cu^{2+} molar ratios of La_2CuO_4-1, La_2CuO_4-2, and La_2CuO_4-Citrate were 0.21, 0.18, and 0.12, respectively. According to the electroneutrality principle, the surface nonstoichiometric oxygen amounts (δ) of the 3DOM-structured La_2CuO_4-1 (i.e., $La_2CuO_{4+\delta}$-1), 3D wormhole-like macroporous La_2CuO_4-2 (i.e., $La_2CuO_{4+\delta}$-2), and nonporous La_2CuO_4-Citrate (i.e., $La_2CuO_{4+\delta}$-Citrate) catalysts were estimated to be 0.087, 0.076, and 0.054, respectively. It has been generally believed that a more amount of nonstoichiometric oxygen is beneficial for the enhancement of catalytic performance in oxidation reactions. Therefore, the 3DOM-structured La_2CuO_4-1 catalyst is expected to outperform the 3D wormhole-like macroporous La_2CuO_4-2 and nonporous La_2CuO_4-Citrate catalysts for the combustion of methane. Such a deduction was confirmed by the catalytic activity data of the three materials (see later).

Fig. 5 shows the H_2-TPR profiles of the La_2CuO_4-1, La_2CuO_4-2, and La_2CuO_4-Citrate catalysts. There were five reduction bands for the two porous catalysts. The reduction bands in the low-temperature range (<500 °C) were due to the stepwise reduction of surface and bulk Cu^{3+} and Cu^{2+} species in different local coordination environments to Cu^{2+} and further to Cu^{+}, whereas those in the high-temperature region (>500 °C) were due to the reduction of Cu^{+} to Cu^{0} [14,22,23]. The onset reduction occurred at a lower temperature over the La_2CuO_4-1 catalyst than over the La_2CuO_4-2 catalyst. The results of quantifying the reduction bands reveal that the H_2 consumption (2.04 mmol/g) of La_2CuO_4-1 was much higher than that (1.35 mmol/g) of La_2CuO_4-2 below 500 °C, but it was lower for the former than for the latter above 500 °C (Table 1). Although the La_2CuO_4-Citrate catalyst gave a higher H_2 consumption (2.60 mmol/g) below 500 °C, it was reduced at higher temperatures (321 and 430 °C) than the two porous catalysts. Therefore, the La_2CuO_4-1 catalyst showed much better low-temperature reducibility than the La_2CuO_4-2 and La_2CuO_4-Citrate catalysts. Such a feature might be related to the discrepancy in their porous structure and oxygen nonstoichiometry. Supposing that all of the copper ions in La_2CuO_4 existed in divalency and in trivalency, the H_2 consumption would be 2.47 and 3.70 mmol/g, respectively. It is apparent that the total H_2 consumption of the as-obtained La_2CuO_4 catalysts fell into the range of 2.54–2.71 mmol/g. This result suggests that there was the co-presence of Cu^{3+} and Cu^{2+} ions in each of the as-prepared La_2CuO_4

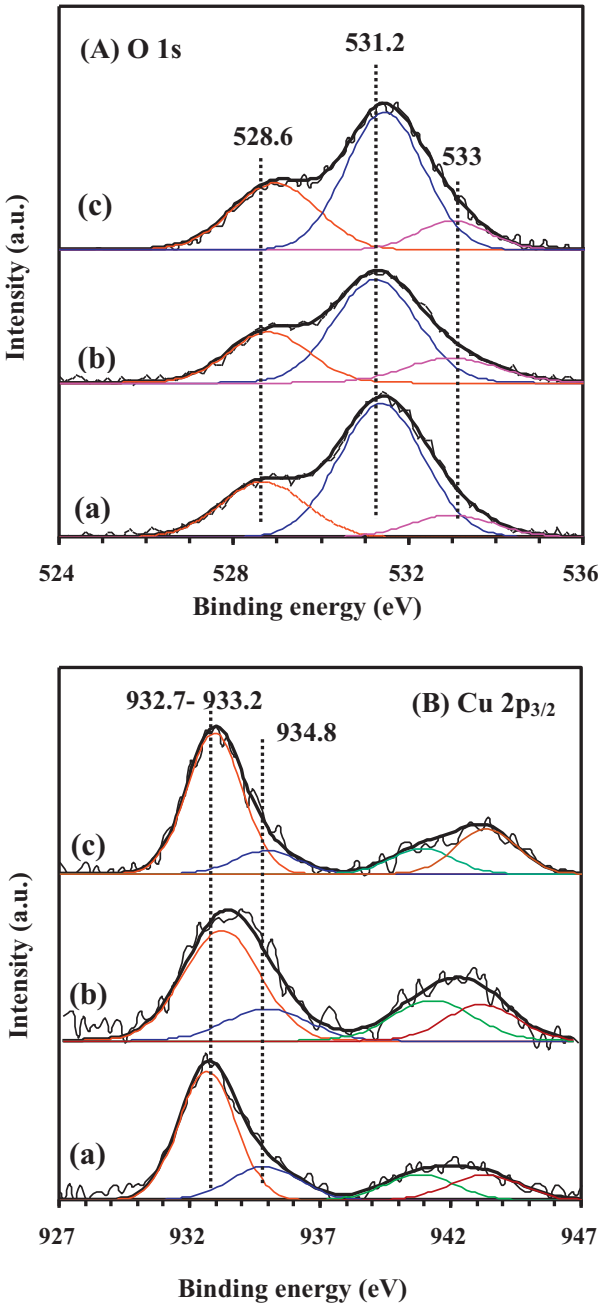

Fig. 4. (A) O 1s and (B) Cu $2p_{3/2}$ XPS spectra of (a) La_2CuO_4-1, (b) La_2CuO_4-2, and (c) La_2CuO_4-Citrate.

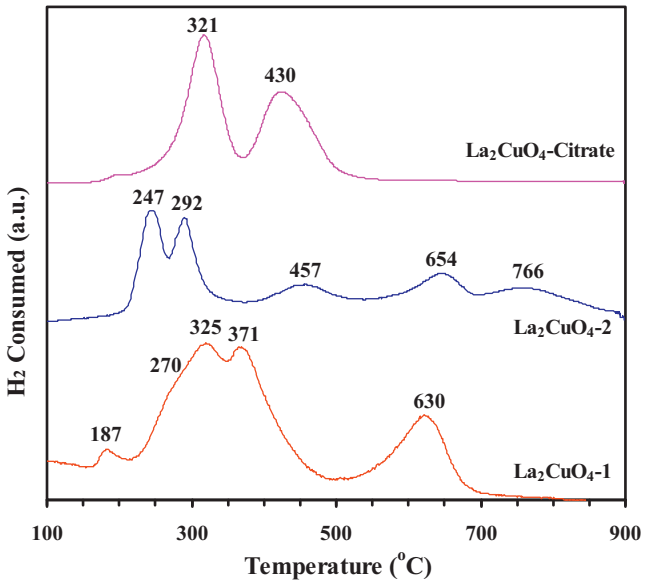

Fig. 5. H_2-TPR profiles of the as-prepared La_2CuO_4 catalysts.

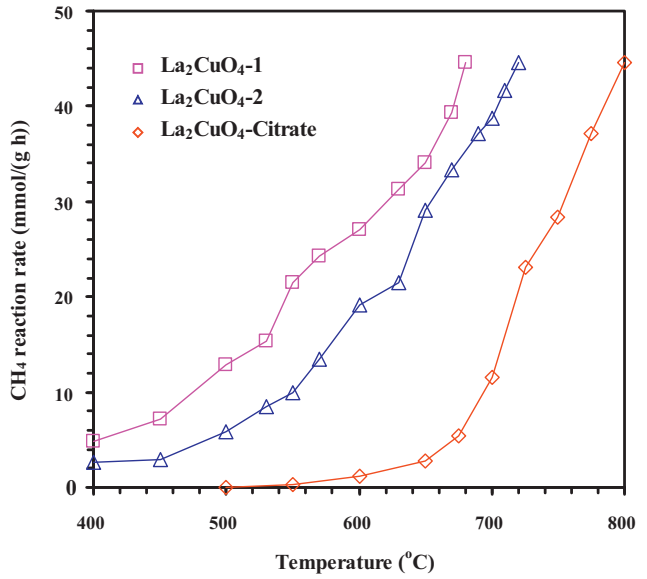

Fig. 6. CH_4 reaction rate as a function of reaction temperature over the La_2CuO_4-1, La_2CuO_4-2, and La_2CuO_4-Citrate catalysts at CH_4/O_2 molar ratio = 1/10 and SV = 50,000 mL/(g h).

catalysts, in good agreement with the results of XPS investigations (Fig. 4).

3.3. Catalytic performance

The result of blank experiment (only quartz sands were loaded in the microreactor) indicated that there was no significant conversion of methane below 770 °C. It demonstrates that no detectable homogeneous reaction took place below 770 °C. Usually, the temperatures ($T_{50\%}$ and $T_{90\%}$) at corresponding methane conversion = 50 and 90% are used to evaluate the activity of a catalyst. From the activity data in Table 1, one can find that the $T_{50\%}$ value (560 °C) was much lower over La_2CuO_4-1 than that (630 °C) over La_2CuO_4-2, and the $T_{90\%}$ value was lower by 33 °C over the former as compared to that over the latter. Apparently, the 3DOM-structured La_2CuO_4-1 catalyst outperformed the 3D wormhole-like macroporous La_2CuO_4-2 catalyst. From Table 1, one can also see that the two porous La_2CuO_4 catalysts were much superior in catalytic performance to the nonporous La_2CuO_4-Citrate catalyst. It is more appropriate to use the reaction rate to compare the catalytic performance of different materials. Fig. 6 shows the methane reaction rate as a function of temperature over the La_2CuO_4-1, La_2CuO_4-2, and La_2CuO_4-Citrate catalysts at a CH_4/O_2 molar ratio of 1/10 and a SV of 50,000 mL/(g h). It can be clearly seen that CH_4 reaction rate augmented with the rise in reaction temperature, and the two porous materials showed much higher CH_4 reaction rates than the nonporous counterpart. The catalytic performance decreased in the order of La_2CuO_4-1 > La_2CuO_4-2 ≫ La_2CuO_4-Citrate. It is worth pointing out that under similar reaction conditions, the catalytic activity ($T_{50\%}$ = 560 °C and $T_{90\%}$ = 672 °C) over our 3DOM-structured La_2CuO_4-1 catalyst was much better than those ($T_{50\%}$ = 654 °C and $T_{90\%}$ = 800 °C) over $La_{0.9}Cu_{0.1}MnO_3$

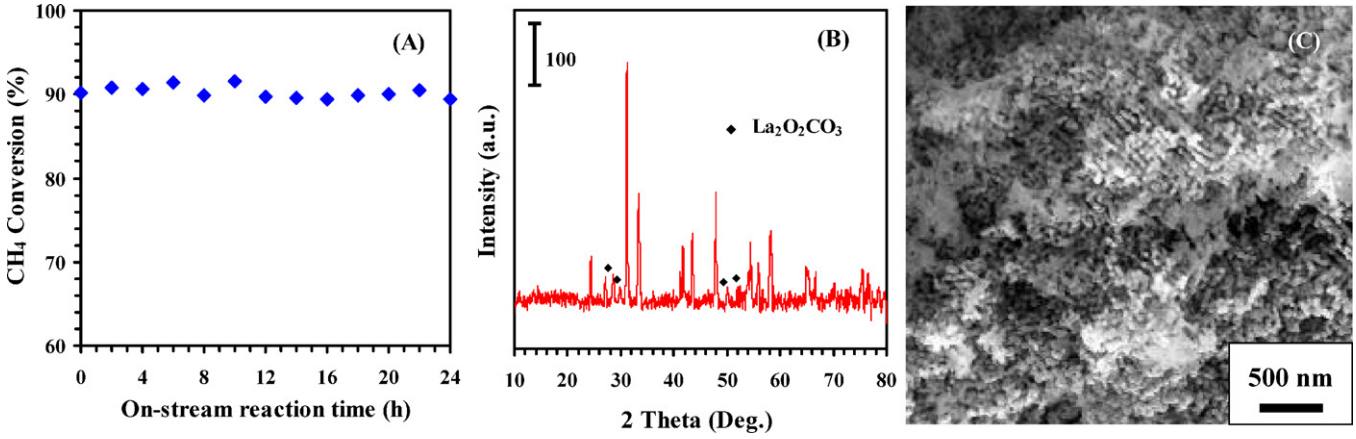

Fig. 7. (A) CH_4 conversion versus on-stream reaction time over the La_2CuO_4-1 catalyst under the conditions of reaction temperature = 672 °C, CH_4/O_2 molar ratio = 1/10, and SV = 50,000 mL/(g h), (B) XRD pattern and (C) SEM image of the La_2CuO_4-1 catalyst after 24 h of on-stream reaction.

[24], ($T_{50\%}$ = 710 °C and $T_{90\%}$ = 770 °C) over 20 wt% $LaMnO_3$/MgO [25], ($T_{50\%}$ = 620 °C and $T_{90\%}$ = 710 °C) over $La_{0.5}Sr_{0.5}MnO_3$ [26], ($T_{50\%}$ = 662 °C and $T_{90\%}$ = 739 °C) over La_2CuO_4 nanorods [14], but inferior to those ($T_{50\%}$ = 365 °C and $T_{90\%}$ = 425 °C) over 1 wt% Pd/ZrO_2 [27] and ($T_{50\%}$ = 520 °C and $T_{90\%}$ = 570 °C) over $La_{0.5}Sr_{0.5}MnO_3$ cubes [28]. Milt et al. [29] reported that $La_2O_2CO_3$ was catalytically active under the conditions of temperature <700 °C and SV = 2700 h^{-1}. Therefore, we believe that the trace amount of $La_2O_2CO_3$ in the La_2CuO_4-1 or La_2CuO_4-2 catalyst would make a minor contribution to the enhancement in catalytic performance of the porous material. In order to examine the catalytic stability, we carried out the lifetime experiment over the La_2CuO_4-1 catalyst within 24 h of on-stream reaction, and recorded the XRD pattern and SEM image of the used La_2CuO_4-1 catalyst. Fig. 7 shows the CH_4 conversion as a function of on-stream reaction time over the La_2CuO_4-1 catalyst under the conditions of reaction temperature = 672 °C, CH_4/O_2 molar ratio = 1/10, and SV = 50,000 mL/(g h), as well as the XRD pattern and SEM image of the used catalyst. It can be found that during the 24-h on-stream reaction no significant catalytic activity loss was observed (Fig. 7A). That is to say, the 3D porous material was catalytically stable. This conclusion was confirmed by the XRD and SEM results, in which no significant changes in crystal phase and XRD peak intensity were detected (Fig. 7B), and the 3D porous structure was also retained in the used La_2CuO_4-1 catalyst (Fig. 7C).

Usually, the combustion of hydrocarbons involves in the activation of C–H bonds by active oxygen species [30,31]. The nature and concentrations of active oxygen species are associated with the defect structure, pore structure, and surface area of a catalyst. As revealed by the XPS results, the 3D porous La_2CuO_4 catalysts possessed nonstoichiometric (extra) oxygen, which would favor the oxidation of methane. The presence of 3D porous structure could facilitate the adsorption and diffusion of methane molecules. It has been believed that catalytic performance is parallel to the BET surface area of a catalyst, especially in the complete oxidation of hydrocarbons and oxygenates [32]. Such a trend coincides with the catalytic activity sequence of La_2CuO_4-1 (46 m^2/g) > La_2CuO_4-2 (39 m^2/g) ≫ La_2CuO_4-Citrate (2.1 m^2/g) obtained in the present work. As demonstrated by the H_2-TPR results, the 3DOM-structured La_2CuO_4-1 catalyst showed much better low-temperature reducibility than the 3D macroporous La_2CuO_4-2 and La_2CuO_4-Citrate catalysts, which might be due to the discrepancy in the porous structure and oxygen nonstoichiometry of these materials. Taking into account the above parameters and by comparing the catalytic activities of the as-prepared La_2CuO_4 catalysts, we hence conclude that the excellent catalytic performance of La_2CuO_4-1 was associated with the factors, such as high surface area, good low-temperature reducibility, and developed 3DOM structure.

4. Conclusion

By using the PMMA-templating strategy with nitrates of lanthanum and copper as metal source in a methanol and ethylene glycol mixed solution and after calcination at various atmospheres, one could prepare 3DOM-structured La_2CuO_4-1 in the presence of citric acid and 3D wormhole-like macroporous La_2CuO_4-2 in the absence of citric acid. In addition to the presence of a trace amount of $La_2O_2CO_3$ phase, the La_2CuO_4-1 and La_2CuO_4-2 catalysts were orthorhombic in crystal structure and possessed rather high surface areas (39–46 m^2/g). The calcination procedure (first in N_2 flow at 700 °C and then in air flow at 300 °C and 800 °C, respectively) was a key step in generating the 3D porous structure of La_2CuO_4. The XPS results indicate that both catalysts were of oxygen overstoichiometry. The low-temperature reducibility of La_2CuO_4-1 was better than those of La_2CuO_4-2 and La_2CuO_4-Citrate. The 3D porous La_2CuO_4 materials showed good catalytic activities for the combustion of methane. Under the conditions of CH_4/O_2 molar ratio = 1/10 and SV = 50,000 mL/(g h), the La_2CuO_4-1 catalyst outperformed the La_2CuO_4-2 and La_2CuO_4-Citrate catalysts, and a CH_4 conversion of 90% could be achieved at 672 °C (reaction rate = ca. 40 mmol/(g h)) over the former catalyst. Based on the above results, we conclude that the main factors, such as higher surface area, better low-temperature reducibility, and developed 3DOM structure, might contribute to the excellent catalytic performance of La_2CuO_4-1.

Acknowledgments

This work was supported by the Scientific Research Key Program of Beijing Municipal Commission of Education (Grant No. KZ200610005004), the <NSF of China (Grant Nos. 20973017 and 21077007), the “863” Key Program of Ministry of Science and Technology of China (Grant No. 2009AA063201), the NSF of Beijing Municipality (Grant No. 2102008), the Creative Research Foundation of Beijing University of Technology (Grant Nos. 00500054R4003 and 005000543111501), and the Creative Research Team of Beijing Education Committee (Grant Nos. PHR200907105, PHR201007105, and PHR201107104). We also thank Prof. Hong He (State Key Laboratory of Environmental Chemistry and Ecotoxicology, Research Center for Eco-Environmental Sciences, Chinese Academy of Sciences) for his valuable discussion on the experimental data.

References

[1] G.L. Flem, G. Demazeau, P. Hagenmuller, J. Solid State Chem. 44 (1982) 82–88.
[2] M. Al Daroukh, V.V. Vashook, H. Ullmann, F. Tietz, I. Arual Raj, Solid State Ionics 158 (2003) 141–150.
[3] A.K. Ladavos, P.J. Pomonis, J. Chem. Soc., Faraday Trans. 87 (1991) 3291–3297.
[4] H.X. Dai, C.F. Ng, C.T. Au, J. Catal. 197 (2001) 251–266.
[5] M. Sadakane, C. Takahashi, N. Kato, H. Ogihara, Y. Nodasaka, Y. Doi, Y. Hinatsu, W. Ueda, Bull. Chem. Soc. Jpn. 80 (2007) 677–685.
[6] M. Sadakane, T. Horiuchi, N. Kato, C. Takahashi, W. Ueda, Chem. Mater. 19 (2007) 5779–5785.
[7] M. Sadakane, T. Asanuma, J. Kubo, W. Ueda, Chem. Mater. 17 (2005) 3546–3551.
[8] E.O. Chi, Y.N. Kim, J.C. Kim, N.H. Hur, Chem. Mater. 15 (2003) 1929–1931.
[9] H.N. Li, L. Zhang, H.X. Dai, H. He, Inorg. Chem. 48 (2009) 4421–4434.
[10] H.N. Li, H.X. Dai, H. He, J. Sci. Conf. Proc. 1 (2009) 186–189.
[11] J.R. Niu, J.G. Deng, W. Liu, L. Zhang, G.Z. Wang, H.X. Dai, H. He, X.H. Zi, Catal. Today 126 (2007) 420–429.
[12] J.G. Deng, Y. Zhang, H.X. Dai, L. Zhang, H. He, C.T. Au, Catal. Today 139 (2008) 82–87.
[13] J.G. Deng, H.X. Dai, Y.X. Liu, H.Y. Jiang, L. Zhang, G.Z. Wang, Environ. Sci. Technol. 44 (2010) 2618–2623.
[14] L. Zhang, Y. Zhang, H.X. Dai, J.G. Deng, L. Wei, H. He, Catal. Today 153 (2010) 143–149.
[15] J.G. Deng, L. Zhang, H.X. Dai, H. He, C.T. Au, Appl. Catal. B 89 (2009) 87–96.
[16] A.N. Shirsat, M. Ali, K.N.G. Kaimal, S.R. Bharadwaj, D. Das, Thermochim. Acta 399 (2003) 167–170.
[17] H. Song, J. Yang, J. Zhao, L. Chou, Chin. J. Catal. 31 (2010) 21–23.
[18] J. Martynczuk, M. Arnold, H. Wang, J. Caro, A. Feldhoff, Adv. Mater. 19 (2007) 2134–2140.
[19] M.W. Roberts, Chem. Soc. Rev. 18 (1989) 451–475.
[20] H.X. Dai, C.F. Ng, C.T. Au, J. Catal. 189 (2000) 52–62.
[21] J.H. Choy, D.Y. Jung, S.J. Kim, Q.W. Choi, G. Demazeau, Physica C 185–189 (1991) 763–764.
[22] J.J. Zhu, Z. Zhao, D.H. Xiao, J. Li, X.G. Yang, Y. Wu, J. Mol. Catal. A 238 (2005) 35–40.
[23] J. Liu, Z. Zhao, C.M. Xu, A.J. Duan, Appl. Catal. B 78 (2008) 61–72.
[24] G. Bulgan, F. Teng, S.H. Liang, W.Q. Yao, Y.F. Zhu, Acta Phys.–Chim. Sin. 23 (2007) 1387–1392.
[25] E.E. Svensson, S. Nassos, M. Boutonnet, S.G. Järås, Catal. Today 117 (2006) 484–490.
[26] S. Ponce, M.A. Peña, J.G.L. Fierro, Appl. Catal. B 24 (2000) 193–205.
[27] S. Guerrero, P. Araya, E.E. Wolf, Appl. Catal. A 298 (2006) 243–253.
[28] S.H. Liang, F. Teng, G. Bulgan, Y.F. Zhu, J. Phys. Chem. C 111 (2007) 16742–16749.
[29] V.G. Milt, R. Spretz, M.A. Ulla, E.A. Lombardo, J.L.G. Fierro, Catal. Lett. 42 (1996) 57–63.
[30] V. Blasin-Aubé, J. Belkouch, L. Monceaux, Appl. Catal. B 43 (2003) 175–186.
[31] M. Alifanti, M. Florea, V.I. Pârvulescu, Appl. Catal. B 70 (2007) 400–405.
[32] K.R. Barnard, K. Foger, T.W. Turney, R.D. Williams, J. Catal. 125 (1990) 265–275.